RSC Advances

COMMUNICATION

Cite this: *RSC Adv.*, 2016, **6**, 2131

Received 26th November 2015
Accepted 18th December 2015

DOI: 10.1039/c5ra25142g

www.rsc.org/advances

Improved cellular infiltration into 3D interconnected microchannel scaffolds formed by using melt-spun sacrificial microfibers†

Zongliang Wang,[ac] Tianlin Gao,[b] Liguo Cui,[a] Yu Wang,[a] Peibiao Zhang*[a] and Xuesi Chen[a]

We report a novel fabrication method using melt-spun sacrificial microfibers to make 3D interconnected microchannel scaffolds for improved cellular infiltration. The uniformly distributed cells in the highly porous microchannel scaffold maintained high cellular viability and glycosaminoglycan secretion indicating the good interconnectivity facilitates the smooth delivery of cells throughout the scaffold and allows sufficient oxygen and nutrient mass transport into the scaffold.

One of the goals of tissue engineering is to create scaffolds with a highly porous structure to meet the needs of mass transfer of oxygen and nutrients for a large number of cells.[1] Scaffolds with ideal inner pore structures are highly demanded for successful tissue regeneration.[2] And such a three-dimensional (3D) scaffold should be able to improve cell proliferation as well as infiltration.

Recently, scaffolds designed to mimic native tissue microstructure are widely used to control the behavior of cells and the formation of stem cell aggregates for tissue engineering.[3,4] Manufacturing techniques such as solvent casting-particulate leaching,[5] gas foaming,[6] phase separation,[7] fibre meshes,[8] rapid prototyping[9] and excimer laser photocuring[10,11] have been used to generate porous scaffolds. To produce scaffolds with desired 3D microarchitecture, sacrificial porogens such as 3D printed polyvinyl alcohol (PVA)[12] and melt-spun shellac microfibers[13,14] were used to fabricate 3D interconnected gelatin hydrogel or polydimethylsiloxane (PDMS) scaffold.

In this paper, we present a new general approach for manufacturing microchannel structured poly(lactide-*co*-glycolide) (PLGA) scaffolds. The method involves melt-spun sucrose microfibers as a sacrificial porogen combined with phase separation. Sucrose is an ideal material because its water solubility and non-toxic to human body. Its high melting temperature (about 186 °C) makes it feasible for melt-spinning. PLGA solution is cast around the sacrificial microfibers and freezing-dried for sublimation of the solvent. Then the microfibers are dissolved, leaving behind a 3D interconnected microchannel PLGA scaffold with good interconnectivity. The microarchitecture, porosity, mechanical property, as well as cell attachment, proliferation and infiltration are evaluated.

The goal of tissue engineering is creation of volumetric tissues and organs *in vitro*. To achieve it, the development of a three-dimensional network throughout the constructs is essential for supplying oxygen and nutrients to all of the cells in the constructs. To keep these seeded cells alive, medium or blood should be perfused into the scaffold as soon as possible after seeding.[15] However, the space and distance between fiber adjacent surfaces in our previously fabricated fibrous scaffold[16] is large, cells only attach and stretch on the 2-D surfaces of 3-D fibrous scaffold. According to literatures, when adjacent surfaces are nearby, cell bridging between surfaces occurs.[17–19] On the other hand, scaffold with 3-D interconnected fibrous network has been fabricated by phase separation.[20] However, one drawback of the scaffolds is the lack of interconnected macropores.[17] In this study, ESEM images of both PLGA porous and microchannel scaffolds (80 wt% sacrificial microfibers) are shown in Fig. 2. The porous scaffold (Fig. 2a) showed ordinary porous microstructure. The large pores in the scaffold were homogeneously distributed and interconnected with each other. Whereas the microchannel scaffold presented more interconnected micropores throughout the scaffold and channel-like structures resulted by the sacrificial microfibers appeared (Fig. 2c and d). It's no doubt that this will be beneficial for cell penetration deep inside the scaffold and diffusion of oxygen and nutrient throughout the channel network.

This new producible technique for fabricating 3D tissue engineering scaffolds using microchannel structures combined with phase separation is simple and involves melt-spun

[a]*Key Laboratory of Polymer Ecomaterials, Changchun Institute of Applied Chemistry, Chinese Academy of Sciences, Changchun 130022, P. R. China. E-mail: zhangpb@ciac.ac.cn; Fax: +86 431 85262058; Tel: +86 431 85262058*

[b]*School of Public Health, Jilin University, Changchun, 130021, P. R. China*

[c]*University of Chinese Academy of Sciences, Beijing 100039, P. R. China*

† Electronic supplementary information (ESI) available. See DOI: 10.1039/c5ra25142g

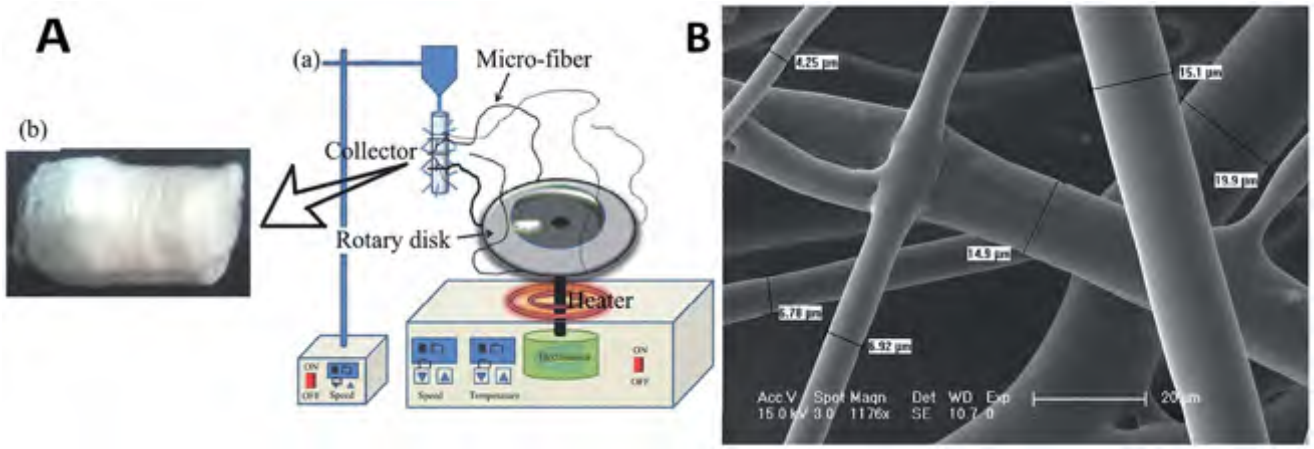

Fig. 1 (A) Schematic diagrams (a) showing melt-spinning method to fabricate microfibers (b).[16] (B) ESEM images of sacrificial sucrose microfibers.

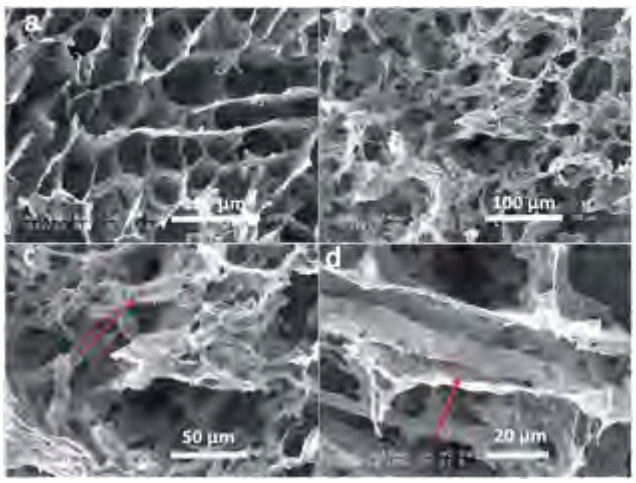

Fig. 2 ESEM images of PLGA porous scaffold (a), microchannel scaffold (b–d) by 80 wt% sacrificial microfibers. The red arrow in (c) and (d) indicate pore structure formed by sacrificial microfiber within the matrix.

sacrificial sucrose microfibers as porogens, which defines the microchannels and highly interconnected structure within the scaffold (Fig. 2b–d). In our previous study, melt-spun fibers were produced to prepare nano/micro-fibrous scaffolds for bone defect repair (Fig. 1A).[16] The microfiber diameters defining the resulting channel diameters can be determined by the melt-spinning temperature and rotational rate. The melting point of sucrose is about 186 °C, so the parameters in this study was set up as 200 °C and the rotational rate is 1000 rpm. The diameters of sucrose fibers are mainly several micrometers to about 20 μm (Fig. 1B). Sucrose fibers were uniformly distributed in the scaffold from the ESEM image of microchannel scaffold (Fig. 2b). Combining with our previous study, it can be seen that the sacrificial fibers of varying sizes ranging from tens of microns to tens of nanometers can be obtained. Hence the sacrificial structures of varying sizes within the microchannel scaffold seems to be realistic.

Pore architecture has been proved to be a critical factor affecting the properties of porous scaffolds and the cell behaviors, as well as cell functions.[21,22] So, a scaffold with appropriate pore structures, such as high porosity, optimal pore size and good interconnectivity, is highly demanded for tissue regeneration.[2] In this study, the porosity of the scaffolds increased gradually as shown in Fig. 3a, benefiting from the solvent sublimation and specifying the infill amount of the sacrificial microfibers. The macropore size of porous scaffold and microchannel scaffold was (52.6 ± 20.4) μm and (65.1 ± 15.4) μm, respectively. Furthermore, a large number of micropores appeared in the microchannel scaffold due to addition of the

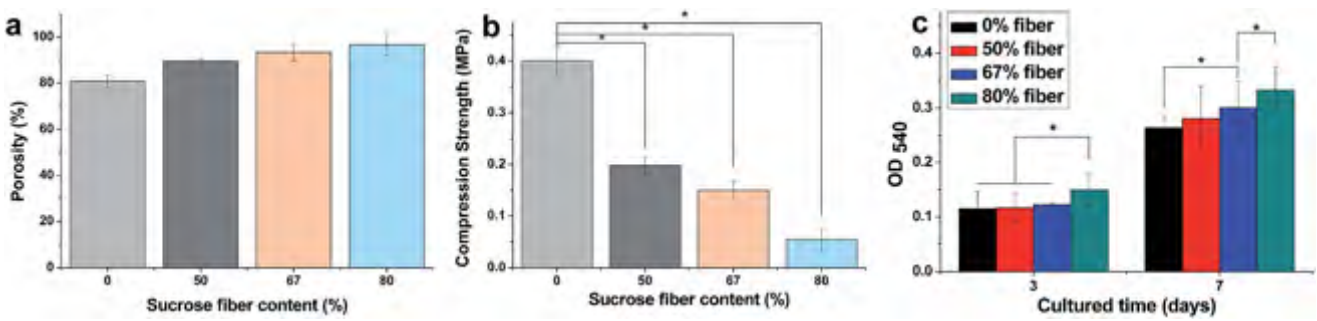

Fig. 3 The porosity, compressive strength of scaffolds and chondrocytes proliferation in the scaffolds for 3 and 7 days.

 This journal is © The Royal Society of Chemistry 2016

sacrificial fibers which might be affect the formation of ice crystals in the frozen process.[23] So the substantial macro and micropores would benefit for cell ingrowth, infiltration and mass transport. The channel-like structure and substantial micropores could bring high surface area within the microchannel scaffold volume. A highly available surface area in a scaffold can provide high ligand density for initial cell attachment and proliferation.[24] As shown in Fig. 3b, the compressive strength of microchannel scaffolds fabricated with different amount of sacrificial microfibers significantly decreased compared to the porous scaffold ($p < 0.05$). The relationship between compressive strength and porosity is expected to be inverse because of a higher porosity should be meant less material to resist applied load and therefore has a lower compressive strength.[12] Fig. 3c shows that cell amount increased over time, indicating the cells proliferated in all scaffolds. The cell amount in microchannel scaffolds was significantly higher than that in porous scaffold when the cells were cultured for 3 and 7 days, especially for the 80 wt% sacrificial microfibers group ($p < 0.05$), suggesting the cells proliferated more quickly in microchannel scaffolds than did in porous scaffold during cell culture.

A spatial distribution of cells throughout porous scaffolds is desirable for homogenous ECM deposition and uniform tissue regeneration.[25] It remains a challenge to maintain viable cells within the deep inner of engineered tissue constructs due to insufficient oxygen and nutrient.[26] To meet this need, a homogeneous cell distribution should be maintained inside the porous scaffold structure.[27] Even if it has the lowest compressive strength, the microchannel scaffold with the highest porosity (96.67%) was chosen for culturing cells and definitely enabled better mass transport, cell attachment and infiltration. In order to visualize cell infiltration and distribution inside the scaffold, the cell nuclei stained scaffolds by DAPI were imaged at the cross section (Fig. 4a and b). Cells were seen to be uniformly distributed throughout deep inside the microchannel scaffold unlike that only in the surface layer of the porous scaffold. The achieved homogeneity can be attributed to the microchannels and highly porous structures with good interconnectivity in the whole microchannel scaffold which facilitates the smooth delivery of cells throughout the scaffold and allows sufficient oxygen and nutrient mass transport into the scaffold. Thus at the end of the culture period, cells were seen to be uniformly distributed throughout the microchannel scaffold. Results from ESEM clearly showed good cell morphology and attachment to the scaffold surface (Fig. 4c). Cell functionality was assessed by measuring GAG secretion of cells in microchannel scaffold (Fig. 4d). Toluidine blue staining indicates that the cells were uniformly distributed and able to maintain their function in the presented 3D interconnected microchannel scaffold.

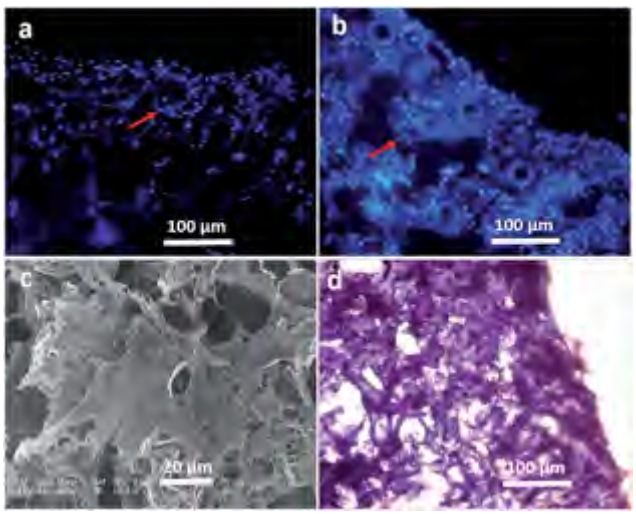

Fig. 4 Spatial cell distribution of chondrocytes in porous scaffold (a) and microchannel scaffold (b). Cell nuclei were stained by DAPI and observed under a fluorescence microscope. (c) Adhesion of chondrocytes in microchannel scaffold for 7 days. (d) Toluidine blue staining of chondrocytes cultured in microchannel scaffold for 7 days.

Conclusions

In this study, we have demonstrated a new technique for fabricating scaffolds using melt-spun sacrificial sucrose microfibers combined with phase separation leading to 3D interconnected microchannel scaffolds. By observing the biological activity of the chondrocytes in the scaffold we conform that along with maintaining very high cellular viability the microchannel scaffold could also support high level of cellular GAG secretion. The microchannels and 3D interconnected structure facilitate the smooth delivery of cells throughout the scaffold and allows sufficient oxygen and nutrient mass transport into the scaffold. In conclusion, the described process is simple, producible with cell culture and infiltration.

Acknowledgements

This research was financially supported by National Natural Science Foundation of China (Projects. 51403197, 51473164, 51273195, and 51203152), the Ministry of Science and Technology of China (International Cooperation and Communication Program 2014DFG52510), the Joint funded program of Chinese Academy of Sciences and Japan Society for the Promotion of Science (GJHZ1519) and the Program of Scientific Development of Jilin Province (20130201005GX).

Notes and references

1 R. Langer, *Adv. Mater.*, 2009, **21**, 3235–3236.
2 H. Mao, N. Kawazoe and G. Chen, *Colloids Surf., B*, 2015, **126**, 63–69.
3 L. E. Freed, G. C. Engelmayr Jr, J. T. Borenstein, F. T. Moutos and F. Guilak, *Adv. Mater.*, 2009, **21**, 3410–3418.
4 A. Khademhosseini and N. A. Peppas, *Adv. Healthcare Mater.*, 2013, **2**, 10–12.
5 R. Huang, X. M. Zhu, H. Y. Tu and A. Wan, *Mater. Lett.*, 2014, **136**, 126–129.
6 C. D. Ji, N. Annabi, M. Hosseinkhani, S. Sivaloganathan and F. Dehghani, *Acta Biomater.*, 2012, **8**, 570–578.

7 E. Rezabeigi, P. M. Wood-Adams and R. A. L. Drew, *Polymer*, 2014, **55**, 6743–6753.

8 S. T. M. Hirota, I. Sato, T. Ozawa, T. Iwai, A. Ametani, M. Sato, Y. Noishiki, T. Ogawa, T. Hayakawa and I. Tohnai, *Biomaterials*, 2016, **75**, 223–236.

9 F. J. Martinez-Vazquez, M. V. Cabanas, J. L. Paris, D. Lozano and M. Vallet-Regi, *Acta Biomater.*, 2015, **15**, 200–209.

10 S. Beke, R. Barenghi, B. Farkas, I. Romano, L. Korosi, S. Scaglione and F. Brandi, *Mater. Sci. Eng., C*, 2014, **44**, 38–43.

11 B. Farkas, I. Romano, L. Ceseracciu, A. Diaspro, F. Brandi and S. Beke, *Mater. Sci. Eng., C*, 2015, **55**, 14–21.

12 S. Mohanty, L. B. Larsen, J. Trifol, P. Szabo, H. V. R. Burri, C. Canali, M. Dufva, J. Emneus and A. Wolff, *Mater. Sci. Eng., C*, 2015, **55**, 569–578.

13 L. M. Bellan, M. Pearsall, D. M. Cropek and R. Langer, *Adv. Mater.*, 2012, **24**, 5187–5191.

14 A. Jacoby, R. C. Hooper, J. Joyce, R. Bleeker, O. A. Asanbe, H. L. Osoria, T. Elshazly and J. A. Spector, *Surg., Gynecol. Obstet.*, 2014, **219**, S140–S141.

15 T. Takei, N. Kishihara, S. Sakai and K. Kawakami, *Biochem. Eng. J.*, 2010, **49**, 143–147.

16 L. G. Cui, N. Zhang, W. W. Cui, P. B. Zhang and X. S. Chen, *J Bionic Eng*, 2015, **12**, 117–128.

17 R. Ng, R. Zang, K. K. Yang, N. Liu and S. T. Yang, *RSC Adv.*, 2012, **2**, 10110–10124.

18 R. Ng, J. S. Gurm and S. T. Yang, *Biotechnol. Prog.*, 2010, **26**, 239–245.

19 Y. Yang, S. Basu, D. L. Tomasko, L. J. Lee and S. T. Yang, *Biomaterials*, 2005, **26**, 2585–2594.

20 Y. Xu, D. Zhang, Z. L. Wang, Z. T. Gao, P. B. Zhang and X. S. Chen, *Chin. J. Polym. Sci.*, 2011, **29**, 215–224.

21 Q. Zhang, H. X. Lu, N. Kawazoe and G. P. Chen, *Acta Biomater.*, 2014, **10**, 2005–2013.

22 C. M. Murphy, M. G. Haugh and F. J. O'Brien, *Biomaterials*, 2010, **31**, 461–466.

23 K. Nakagawa, N. Thongprachan, T. Charinpanitkul and W. Tanthapanichakoon, *Chem. Eng. Sci.*, 2010, **65**, 1438–1451.

24 F. J. O'Brien, B. A. Harley, I. V. Yannas and L. J. Gibson, *Biomaterials*, 2005, **26**, 433–441.

25 M. M. C. G. Silva, L. A. Cyster, J. J. A. Barry, X. B. Yang, R. O. C. Oreffo, D. M. Grant, C. A. Scotchford, S. M. Howdle, K. M. Shakesheff and F. R. A. J. Rose, *Biomaterials*, 2006, **27**, 5909–5917.

26 Q. C. Zhang, H. Y. Luo, Y. Zhang, Y. Zhou, Z. Y. Ye, W. S. Tan and M. D. Lang, *Mater. Sci. Eng., C*, 2013, **33**, 2094–2103.

27 H. J. Lee, S. H. Ahn, L. J. Bonassar, W. Chun and G. H. Kim, *Tissue Eng., Part C*, 2013, **19**, 784–793.

This journal is © The Royal Society of Chemistry 2016